Generating Transferrable Adversarial Examples via Local Mixing and Logits Optimization for Remote Sensing Object Recognition

Chun Liu[a], Hailong Wang[b], Bingqian Zhu[b], Panpan Ding[b], Zheng Zheng[c], Tao Xu[b,*], Zhigang Han[a] and Jiayao Wang[a]

[a]State Key Laboratory of Spatial Datum, College of Remote Sensing and Geoinformatics Engineering, Henan University, Zhengzhou, 450046, China
[b]School of Computer and Information Engineering, Henan University, Kaifeng, 475004, China
[c]School of Automation Science and Electrical Engineering, Beihang University, Beijing, 100091, China

ARTICLE INFO

Keywords:
adversarial attacks
adversarial transferability
model robustness
object recognition
remote sensing

ABSTRACT

Deep Neural Networks (DNNs) are vulnerable to adversarial attacks, posing significant security threats to their deployment in remote sensing applications. Research on adversarial attacks not only reveals model vulnerabilities but also provides critical insights for enhancing robustness and resilience. Although current mixing-based strategies have been proposed to increase the transferability of adversarial examples, they either perform global blending or directly exchange a region in the images, which may destroy the global semantic features of the images and mislead the optimization direction of adversarial examples. Furthermore, their reliance on cross-entropy loss for perturbation optimization leads to gradient diminishing during iterative updates, directly compromising adversarial example quality. To address these limitations, we focus on non-targeted attacks and propose a novel framework via local mixing and logits optimization for generating transferable adversarial examples in remote sensing object recognition. First, we present a local mixing strategy to generate diverse yet semantically consistent inputs during the generation of adversarial examples. Different from the typical MixUp method which globally blends two images and the MixCut method which stitches different images together, the proposed local mixing method merely blends local regions of two images to preserve as much of the global semantic information as possible. Second, we adapt the logit loss from target attacks to non-target attack scenarios, to mitigate the gradient vanishing problem inherent to cross entropy loss. Third, we have also applied a perturbation smoothing loss to suppress excessively high-frequency noise to further enhance the transferability of adversarial examples generated. Extensive experiments on FGSCR-42 and MTARSI datasets demonstrate superior performance over 12 state-of-the-art methods across 6 surrogate models. Notably, with ResNet as the surrogate model on MTARSI, our method achieves a 17.28% average improvement in black-box attack success rate.

1. Introduction

With the rapid development of earth observation technology, a massive number of high-resolution remote sensing images are being collected from satellites and aerial platforms. These data play a crucial role in a wide range of applications, including natural disaster monitoring, urban planning, forest resource survey, and military reconnaissance. Effectively analyzing such vast quantities of remote sensing images has therefore become a pressing issue. In particular, remote sensing object recognition is to identify the type of an object in the image scenes, which provides essential support for higher-level applications such as content-based remote sensing image retrieval and remote sensing target detection.

Due to the powerful feature extraction ability, deep neural networks (DNNs) are widely applied to remote sensing object recognition [1; 2; 3]. However, DNNs are vulnerable to adversarial attacks during real-world deployment. By crafting adversarial examples which involve subtle and nearly imperceptible changes to normal examples, attackers can easily mislead the DNN models to produce incorrect results [4]. These attacks pose serious threats to system reliability and security, particularly in critical remote sensing applications where accurate interpretation is essential for decision-making. Studying adversarial attacks on DNN models for remote sensing object recognition is therefore crucial, as it not only reveals vulnerabilities but also provides critical insights for enhancing model robustness and resilience.

According to the attacker's knowledge of the target model, adversarial attacks can be categorized into white-box attacks [5], [6], [7] and black-box attacks [8], [9], [10], [11], [12], [3], [13], [14], [15], [16]. White-box attacks refer to scenarios where the attackers have complete knowledge of the model's architecture and parameters. The attackers can directly utilize these information to compute the model's gradients and generate adversarial examples with strong attack capabilities. In contrast, black-box attacks assume that the attackers have no access to the internal information of the target model and can only infer the model's behavior through input-output queries, making them more challenging. In real-world scenarios, black-box attacks are of greater practical significance because most models deployed in real environments do not expose their internal structures, and attackers usually cannot directly access the model parameters. According to the attacker's objective, adversarial attacks can also be categorized into targeted [17] [18] and non-targeted attacks. Targeted attacks aim to mislead the model

*Corresponding author.
liuchun@henu.edu.cn (C. Liu); zhengz@buaa.edu.cn (Z. Zheng); txu@henu.edu.cn (T. Xu); zghan@henu.edu.cn (Z. Han); wjy@henu.edu.cn (J. Wang)
ORCID(s):

into classifying inputs as a specific class, while non-targeted attacks cause the model to misclassify inputs without any predefined target. We focus on the non-targeted black-box attacks in this study, which play a significant role in revealing model vulnerabilities.

To achieve black-box attacks, transferable attacks offer an effective approach. The basic idea is to craft adversarial examples on an accessible substitute model and leverage their transferability across different models so that they can also fool the target black-box model. When generating transferable adversarial examples, traditional transferable attack methods often suffer from overfitting to the substitute model and lead to degraded performance on other models. To address the overfitting problem, input transformation-based methods [8], [9], [10], [11], [12], [3] have emerged in recent years, enhancing input diversity through data augmentation during adversarial examples generation. By averaging the gradients over multiple transformed inputs, these methods mitigate overfitting and improve the transferability of the adversarial examples generated.

While existing research mainly focuses on adversarial attacks in the field of natural images, relevant findings indicate that such threats also exist in the field of remote sensing [19]. For example, to interfere with the models in the scene classification tasks [20], researchers have designed different attack methods through input transformations [21], multimodal data [22], and other techniques. However, existing attack methods fail to fully leverage the unique characteristics of remote sensing images. As shown in Figure 1, remote sensing images are characterized by highly complex and diverse backgrounds, ranging from urban landscapes to natural environments. Traditional input transformation methods augment individual images through operations like rotation, scaling, or cropping, essentially generating variations of the same scene content. This fundamentally limits adversarial example generalization across models. While several mixing-based strategies, such as MixUp/MixCut [23], and Admix [24], have been proposed to increase input diversity, they either perform global blending or directly exchange a region in the images, which may destroy the global semantic features of the images and reduce the quality of generated adversarial examples. Furthermore, these methods still use the typical cross entropy loss to optimize the perturbation, which suffers from gradient diminishing [18] during iterative gradient updates. That is, the loss gradient concerning the input diminishes toward zero as iterations increase. Since transferable attacks rely on substitute model gradients to update perturbations, this issue directly compromises adversarial example quality.

To address these limitations, we in this paper focus on remote sensing object recognition task and propose a novel method via local mixing and logits optimization for generating highly transferrable adversarial examples. First, we present a local mixing strategy to generate diverse yet semantically consistent inputs during the generation of adversarial examples. Different from the typical MixUp method [23] which globally blends two images and the MixCut method [23] which directly stitches different images together, the proposed local mixing method merely blends local regions of two images to preserve as much of the global semantic information as possible. Second, we introduce a logits-based optimization specifically adapted for non-targeted attacks in object recognition. While previous work [25] applied logit loss in targeted attack scenarios, we reformulate it for non-targeted attacks by directly minimizing the logits of the true class. Fundamentally different from traditional cross-entropy loss optimization, it bypasses the softmax operation that causes gradient vanishing [26], thereby maintaining stronger gradient signals throughout the iterative optimization process—a critical factor for transferable adversarial example generation. Third, acknowledging that excessively high-frequency perturbation components impair transferability[15], we have also applied a perturbation smoothing loss which uses a mean filter to suppress excessive high-frequency components to further enhance transferability across heterogeneous DNN architectures. The main contributions of this paper are as follows:

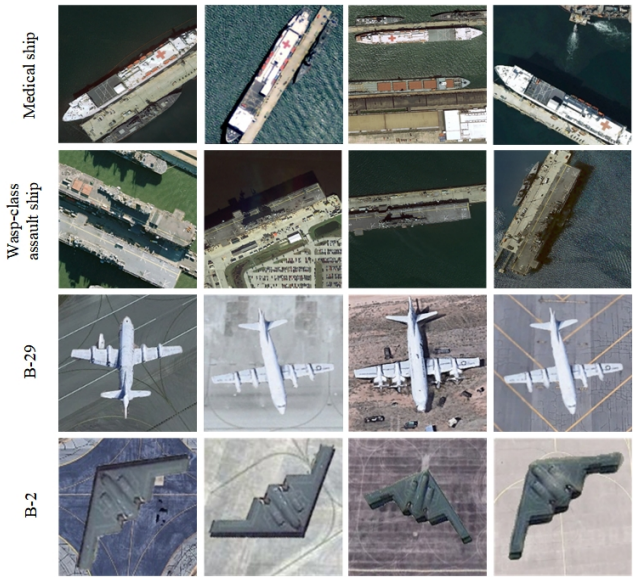

Figure 1: Remote sensing images from FGSCR-42 and MTARSI datasets demonstrate the complex background diversity and semantic consistency within each class category.

1. We propose a local mixing strategy to alleviate overfitting in adversarial example generation for remote sensing object recognition. By merely blending the random regions of two images, our method leverages background diversity and generates diverse yet semantically consistent inputs.

2. We design a novel untargeted attack loss based on logits optimization. Unlike cross-entropy loss, our approach directly minimizes the true-class logits to avoid gradient vanishing, and integrates a perturbation-smoothing loss to suppress high-frequency noise, leading to more transferable adversarial examples across diverse architectures.

3. We conduct extensive experiments on two datasets, showing that our method consistently outperforms existing approaches. For example, on the MTARSI dataset with

ResNet as the substitute model, we achieve up to 17.28% average improvement in attack success rate.

The remainder of this paper is structured as follows. Section 2 briefly introduces the related work. Section 3 details the proposed method. Section 4 describes the datasets, the design and the results of the experiments. Finally, the conclusions are in section 5.

2. Related work

2.1. Adversarial attacks

Adversarial attacks are typically divided into two main categories: white-box attacks and black-box attacks. This classification is based on the extent to which the attacker has control over the target model [27]. In white-box attacks, the attacker has full access to the target model's architecture and parameters, allowing them to exploit the model's weaknesses to carefully design perturbations that achieve the desired attack outcome. Classic white-box attack methods include the Fast Gradient Sign Method (FGSM) [4] and Projected Gradient Descent (PGD) [28]. These methods optimize input perturbations using the gradient information of the target model, causing the model to make incorrect predictions.

In practical applications, since attackers typically cannot access detailed information about the target model, black-box attacks are more realistic and pose a significant threat to the application of deep neural networks. Currently, black-box attack methods are divided into two types: query-based attacks and transfer-based attacks. In query-based attacks [29; 30], the attacker repeatedly sends query requests to the target model and generates adversarial examples based on the information provided by the model's feedback. However, due to the need for frequent query operations, these attacks are computationally expensive, particularly when handling large-scale datasets, where query costs can increase significantly. Transfer-based attacks are a viable black-box attack method, where adversarial examples are generated by attacking a substitute white-box model. These adversarial examples are then transferable and can effectively attack the black-box model as well. These classic white-box attack methods like FGSM [4] and PGD [28] do not perform well in transferability. Enhancing the transferability of adversarial examples remains a challenging problem.

In recent years, researchers have proposed various optimization strategies to enhance the transferability of adversarial examples. Liu et al. [14] introduced a method based on the ensemble of multiple substitute models, aiming to improve the transferability of adversarial examples across different models. Dong et al. [13] proposed the Momentum Iterative Method (MIM), an iterative attack method that introduces momentum into the gradient updates to accelerate convergence and effectively enhance the transferability of adversarial examples. Gao et al. [9] proposed PIM, which focuses not on the global image but on the patches of the input images, improving adversarial effectiveness by precisely interfering with these regions. Ding et al. [16] explored a black-box attack method, OSFD, which interferes with intermediate layer features. By amplifying transformed features and separating them from the original features, OSFD improves the transferability of adversarial examples.

Input transformations, as a means of combating overfitting, have also been applied in recent years to improve transferability. Initially, input transformations were primarily focused on the spatial domain, where various transformations were applied to the input data. For example, Xie et al [8] first proposed the Diversity Input Method (DIM), which enhanced the transferability of adversarial examples across different models by applying diverse random transformations to the input images. Guo et al. [31] introduced BSR, which instead of transforming the entire input image, first divides the image into blocks, then performs random shuffling and rotation operations on these blocks. Later, Dong et al. [10] proposed TIM, which optimized the uniformity of input perturbations under spatial translations, making adversarial examples more transferable to target models. Lin et al. [11] proposed SIM, which took advantage of the target model's invariance to input scale changes and enhanced the robustness and transferability of adversarial examples by simulating input images at different scales. Wang et al. [24] introduced Admix, which linearly combines adversarial examples with other randomly selected natural images, simulating the diversity of input distributions and thereby enhancing transferability.

With the deepening of research, the application of input transformations has extended to the frequency domain. Zhang et al. [12] proposed SSA, which aims to enhance the diversity of adversarial examples in the frequency domain through spectral transformations, thereby generating more transferable adversarial examples that can effectively attack various defense models. Unlike natural images, in the field of remote sensing target recognition, researchers have begun to explore more complex transformation strategies by combining the characteristics of remote sensing data. Fu et al. [3] discovered that the key to remote sensing object recognition lies in the features of the target-related regions. To address this, they proposed the SFCoT method, which combines frequency and spatial domain transformations to achieve effective decoupling of the target and background. Subsequently, the method applies block-wise input transformations to the decoupled regions, significantly enhancing the transferability of the model.

2.2. Adversarial defense

Adversarial defense aims to enhance the ability of deep learning models to resist adversarial examples attacks. Existing defense strategies primarily include model optimization, adversarial training, and data preprocessing methods.

In model optimization approaches, the main idea is to improve the robustness of models by modifying the training process or regularizing the model's parameters to better resist adversarial perturbations. Papernot et al. [32] proposed defensive distillation, training models via a distillation algorithm using output probability distributions as new labels. Addepalli et al. [33] introduced a novel Bit Plane Feature

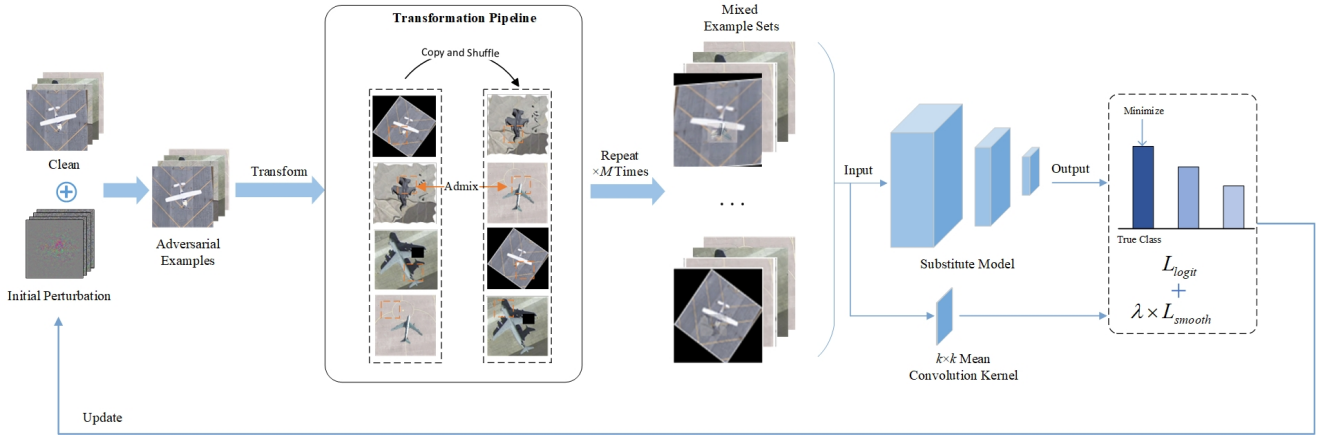

Figure 2: Overview of our proposed method. Adversarial examples are first passed through a transformation pipeline to introduce diversity. Mixed images are passed through a surrogate model to compute logit loss (minimizing true class logit) and smoothing loss via a $k \times k$ mean convolution kernel. We then compute the smooth gradient and combine it with momentum to iteratively update the perturbation.

Consistency (BPFC) regularization method, improving adversarial robustness by constraining consistency across different quantized image representations. Additionally, Liao et al. [34] proposed a high-level representation-guided denoiser, using a U-Net denoising network to remove noise from images and counter adversarial attacks.

Adversarial training was first proposed by Goodfellow et al. [4], utilizing the Fast Gradient Sign Method (FGSM) to generate adversarial examples, which are then mixed with original images for training. Madry et al. [28] improved adversarial training by introducing a Projected Gradient Descent (PGD)-based method. Tramer et al. [35] proposed ensemble adversarial training, using adversarial examples generated from multiple pretrained models to enhance robustness against cross-model adversarial examples. Kannan et al. [36] introduced a logit pairing strategy based on PGD adversarial training, proposing a hybrid mini-batch PGD method. By pairing clean images with adversarial or other clean ones, this approach significantly improves model robustness under both white-box and black-box attacks.

In data preprocessing-based adversarial defense methods, the core idea is to modify the input data in a way that reduces the effect of adversarial perturbations before they reach the model. Guo et al. [37] proposed input transformation techniques such as image scaling, cropping, and compression to eliminate perturbations while preserving useful information. Xie et al. [38] suggested random resizing and padding of images. They also proposed a pixel deflection-based method, perturbing pixel values locally and combining wavelet denoising techniques to effectively reduce damage from pixel shifts and adversarial perturbations. Jin et al. [39] introduced the APE-GAN strategy, utilizing a generator to simultaneously reconstruct adversarial and clean examples.

3. Methodology

3.1. Problem description

Given a target model f, a clean image x, and its true label y, an adversarial attack aims to construct an adversarial example x^{adv} to deceive the model such that:

$$f(x^{adv}) \neq f(x) = y \tag{1}$$

where x^{adv} is generated by adding a small perturbation δ to x, and this perturbation is visually imperceptible to human observers, satisfying

$$\|x^{adv} - x\|_p \leq \epsilon \tag{2}$$

where $\|\cdot\|_p$ denotes the p-norm. Following previous works [13], [8], [10], [11], [12], [3], we adopt the ∞-norm ($p = \infty$). We formulate this optimization problem through Eq. 1, where L is the loss function and ϵ controls the magnitude of the perturbation

$$x^{adv} = \arg\max L, \quad \text{s.t.} \quad \|x^{adv} - x\|_\infty \leq \epsilon \tag{3}$$

3.2. The overview of the proposed method

To address this optimization challenge, we propose a lightweight framework via local mixing and logits Optimization for remote sensing object recognition task, to generate adversarial examples with superior transferability.

Fig. 2 comprehensively illustrates the workflow of our method. Initially, It begins with a batch of clean images and a adversarial perturbation. After adding the clean images with the adversarial perturbation to generate the adversarial examples, a data augmentation operation is randomly selected from Table. 1 and applied to the adversarial examples, creating a set of augmented images. These augmentation operations—including rotation, scaling, and cropping—effectively simulate various real-world image variations. Subsequently, it duplicates this set of augmented images and randomly shuffles their order to create potential

mixing candidates. It then randomly selects rectangular regions within the images and apply the Admix technique to proportionally blend the selected regions of the original set of augmented images with the regions from their shuffled counterparts, generating a mixed image set. Notably, it repeats above transformation process multiple times, each time applying different mixing regions and data augmentation operations. The resulting sets of mixed images and their corresponding labels are concatenated across these diverse transformations and used jointly for gradient computation. This strategy effectively explores a broader perturbation space, significantly enhancing the transferability of the final adversarial examples.

To optimize perturbation search, it develops a composite loss function that combines logit loss with perturbation smoothing loss. Based on the MI-FGSM framework, it utilizes momentum terms to accumulate historical gradient information and reduce optimization noise and fluctuations. Additionally, it incorporates gradient smoothing to reduce overfitting and improve the transferability of adversarial examples. This combination of strategies encourages smoother gradients and more stable update directions, leading to adversarial examples with improved transferability in black-box settings.

The entire algorithm workflow is summarized in Algorithm. 1, which clearly demonstrates the complete process from initialization to final adversarial example generation, including key components such as input transformation, gradient calculation, momentum updates, and adversarial updates during the iteration process. We detail the key components of the proposed method as follows.

3.3. Local mixing based input transformation

In adversarial example generation, data augmentation operations are typically applied to input examples to enhance input diversity and reduce overfitting to the substitute model. However, while enhancing input diversity, these operations may also potentially damage the semantic information of the samples. In extreme cases, a data augmentation operation could destroy key semantic features of the sample and leads to recognition errors in the model. Although such errors are expected by adversarial samples, they are not caused by the perturbation we add. Using the loss generated by this error to optimize the perturbation will lead to deviations in the optimization direction. Therefore, preserving the semantic information of the samples as much as possible during data augmentation is crucial for obtaining high-quality perturbation. To achieve this purpose, we propose a local mixing based input transformation strategy, whose pipeline is illustrated in Fig. 2.

For a batch of images $x = x_1, x_2, \dots, x_b$ which are added by a perturbation, it first applies data augmentation to each image in the batch, generating a transformed image set

$$S_1 = \{T(x_1), T(x_2), \dots, T(x_b)\} \tag{4}$$

where $T(\cdot)$ represents the data augmentation function, which randomly selects one of the transformation operations which are shown in Table 1. These transformations simulate various changes of images in the real world, helping the generated adversarial examples achieve stronger generalization ability.

To further increase the diversity of inputs, we duplicate the augmented image set and apply random shuffling.

$$S_2 = \text{shuffle}(S_1) \tag{5}$$

where shuffle$(\cdot)$ represents the random permutation function. We then adopt a local region-mixing strategy. For each sample index i (where $i = 1, \dots, b$), we randomly select a rectangular region and denote its binary mask as R_i. Within this rectangular region, we blend $S_1[i]$ and $S_2[i]$ using mixing weight $\eta \in (0, 1)$, while keeping the areas outside the rectangular region unchanged from $S_1[i]$.

$$\tilde{x}_i = R_i \odot \left(\eta\, S_1[i] + (1-\eta)\, S_2[i]\right) + (1 - R_i) \odot S_1[i] \tag{6}$$

By shuffling the order of images in S_2, we break the fixed correspondence with S_1, thereby achieving mixing effects between different images to enhance diversity.

3.4. Smoothness-Regularized logit loss

The design of the loss function is crucial for generating effective adversarial perturbations, as it directly determines the quality and stability of the gradients used for optimizing the perturbations. When using the typical cross-entropy loss to optimize the perturbation, the softmax function compresses the logit vector containing arbitrary real numbers into a probability distribution, where each element's value ranges between 0 and 1, and the sum of all elements is 1. When there is one or more extremely large (positive or negative) values in the logit vector, the softmax function enters a saturated state, and its output tends towards a deterministic distribution, leading to an extremely small gradient. This makes it difficult to further optimize the perturbation. Meanwhile, there are usually high-frequency noise in the perturbation. Because different neural networks exhibit varying sensitivities to high-frequency components in the input space, high-frequency noise may drive the attack to exploit model-specific patterns during perturbation optimization. This will harm the transferability of the adversarial examples across different models. To address these issues, we propose a combined loss function that integrates logit loss and perturbation smoothing loss to mitigate gradient vanishing and explicitly penalize high-frequency components. The definitions and roles of these two loss functions are detailed below.

Given an input x and an adversarial perturbation δ, the logit output of the target model f is

$$z = f(x + \delta) \tag{7}$$

where $z \in \mathbb{R}^C$ represents the unnormalized output before softmax (with C being the number of classes). Let z_y denote the logit value of the model for the true class y. The logit loss is defined as

$$L_{logit} = -z_y \tag{8}$$

Table 1
Data Augmentation Strategies in Our Method

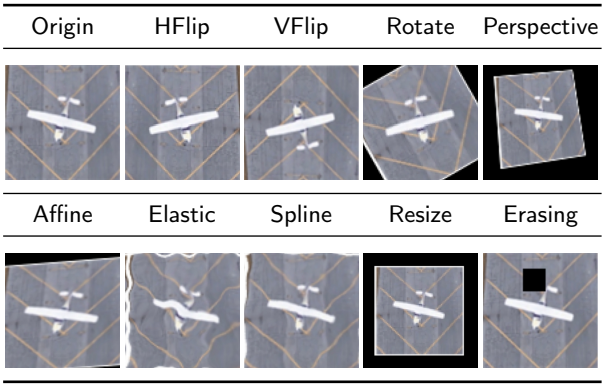

In targeted attack scenarios, the common approach is to maximize the logit value of the target class to strengthen the model's prediction toward that class. In the untargeted attack scenario of this paper, the proposed method minimizes the logit of the true class to weaken the model's confidence in the correct prediction, making misclassification more likely.

Moreover, to prevent the excessive amplification of high-frequency noise during iterative optimization, the proposed method introduces a smoothing loss to smooth the adversarial perturbation and constrain its frequency distribution. Specifically, a low-pass filter is applied to the perturbation δ and the filtered result is taken as a regularization term to limit high-frequency components

$$L_{smooth} = \|\text{LowPassFilter}(x^{adv} - x)\|_1 \tag{9}$$

where LowPassFilter denotes a $k \times k$ mean convolution kernel that attenuates high-frequency components by averaging pixel values within a sliding window.

Ultimately, the logit loss and smoothing loss are combined with specific weights to form a comprehensive loss function.

$$L_{total} = L_{logits} + \lambda L_{smooth} \tag{10}$$

where λ is a hyperparameter that balances the contributions of the loss terms.

3.5. Gradient calculation and perturbations optimization

To obtain smooth gradients and stable update directions, we repeat the above local mixing based input transformation M times, where each transformation generates a batch of images for gradient calculation. Multiple rounds of transformation compensate for the limitations of a single transformation, making the gradient more stable and with stronger generalization capability.

As shown in the formula Eq. 11, we calculate the gradients for each of these M batches and average them to obtain the gradient $\bar{g}_{t+1}$. Based on the gradient, we further adopt a gradient smoothing strategy as shown in Eq. 12 to generate a momentum term to accelerate convergence.

$$\bar{g}_{t+1} = \frac{1}{M} \sum_{m=1}^{M} \nabla_{x_t^{adv}} L_{total}(\tilde{x}_t^{(m)}, y) \tag{11}$$

$$g_{t+1} = g_t + \frac{\bar{g}_{t+1}}{\|\bar{g}_{t+1}\|_1} \tag{12}$$

After computing the gradient, the adversarial example update process is designed as Eq. 13.

$$x_{t+1}^{adv} = Clip_{x,\varepsilon}\{x_t^{adv} + \alpha \cdot sign(g_{t+1})\} \tag{13}$$

To ensure the adversarial perturbations remain imperceptible, we constrain them within an L_∞ ball of radius ε centered at the clean image x. As shown in Eq. 13, each PGD iteration updates the adversarial example and then applies the clipping operation $\text{Clip}_{x,\varepsilon}$ to project x_t^{adv} back into the feasible region $[x - \varepsilon,\ x + \varepsilon]$.

Algorithm 1 Adversarial Example Generation Algorithm

Input: A substitute model f, loss function L, a batch of input images x with label y, supplement α, perturbation budget ε, transformation times M, number of iterations T, and mixing strength η.
Output: A batch of adversarial examples.
$g_0 \leftarrow 0$, $x_0^{\text{adv}} \leftarrow x$
for $t \leftarrow 0$ **to** $T - 1$ **do**
    for $m \leftarrow 1$ **to** M **do**
        Construct a transformed image set and concatenate.
    end for
    Calculate the smooth gradient $\bar{g}_{t+1}$ of the transformed image set by Eq. 11.
    Update the momentum by Eq. 12.
    Update the generated adversarial example x_{t+1}^{adv} based on the sign of g_{t+1}.
end for
return x^{adv}

4. Experiments

4.1. DataSets

The proposed method is tested on the FGSCR-42 [40] and MTARSI [41] datasets. FGSCR-42 is a publicly available dataset specifically designed for fine-grained classification of ships in remote sensing images. It contains 7,776 high-definition remote sensing images, covering 42 different ship categories, including military ships (e.g., aircraft carriers, destroyers) and civilian ships (e.g., cargo ships, cruise ships). These images are primarily collected from Google Earth.

MTARSI is a benchmark dataset for aircraft type recognition in remote sensing images, containing 9,589 high-definition remote sensing images covering 20 aircraft types.

These images are collected from Google Earth and have complex backgrounds, varying spatial resolutions, and differences in pose, location, illumination, and time periods.

Fig. 1 shows some images from the FGSCR-42 and MTARSI datasets. We resize all images to 224×224 pixels. For each class, we randomly divide the dataset into training and testing sets in a 4:1 ratio. After training our model on the training set, we conduct adversarial attack experiments on the test set. The FGSCR-42 dataset can be downloaded from https://github.com/DYH666/FGSCR-42, and MTARSI can be downloaded from https://www.kaggle.com/datasets/aqibriaz/mtarsidataset.

4.2. Model architectures

Using a variety of models with different architectures can help researchers analyze the transferability of adversarial attacks. In this study, we carefully selected six classic deep neural network models which have been widely used in related works to evaluate the effectiveness of adversarial attacks. They are VGG-16[42], VGG-19[42], ResNet-34[43], ResNet-50[43], DenseNet-121[44], and Inception-ResNet-V2[45]. From the relatively shallow VGG to the very deep DenseNet/Inception-ResNet, these models have demonstrated outstanding performance in object recognition and represent key milestones in the development of deep learning. VGG-16 and VGG-19 increase the network depth by stacking multiple 3x3 convolutional layers, emphasizing the importance of depth for performance improvement. ResNet-34 and ResNet-50 introduced residual connections, overcoming the bottleneck of training deep networks. DenseNet-121 employs dense connections to optimize feature reuse and information flow. Inception-ResNet-V2 combines the multi-scale feature extraction of the inception module and the residual connections of ResNet, showcasing the unique advantages of heterogeneous architectures.

By considering a variety of classic models, we ensure that the results of the adversarial attack analysis are not limited to a single architecture. This is of significant importance for developing universal adversarial defense strategies and improving the overall security of deep learning models.

4.3. Comparison methods

To validate the performance of the proposed method, we compared it with several advanced attack methods, including PGD [7], MIM [13], TIM [10], PIM [9], DIM [8], SIM [11], Admix [24], Mixup/MixCut [23], SSA [12], BSR [31], and SFCoT [3]. Specifically, PGD represents the standard iterative attack based on basic gradient updates. MIM introduces momentum optimization to stabilize and guide the update direction. TIM enhances transferability by applying translation-invariant smoothing. PIM focuses on pixel-level attention to refine perturbations. DIM improves robustness through diverse input transformations. SIM leverages scale-invariant transformations to boost attack generalization. Admix, Mixup, and Mixcut are data mixing strategies that generate new adversarial examples by combining multiple inputs. SSA and BSR further explore the spatial and spectral domains to craft more transferable perturbations. Additionally, SFCoT decouples target and background features in the frequency domain for targeted perturbation optimization.

4.4. Implementation details

In our experiments, the target models were trained on the training set, and adversarial attacks were conducted on the test set samples that all models classified correctly. During the generation of adversarial examples, the perturbation constraint ε, step size α, and number of iterations T were set to 16, 1, and 30, respectively. The local mixing based input transformation times M used for gradient computation were set to 25, and the loss weight λ was set to 200. These parameters (ε, α, T) were kept consistent with the settings in SFCoT. In the input transformation phase, the mixing strength η was set to 0.5. Parameters specific to each comparison method followed their recommended configurations. Experiments were conducted in the PyTorch framework with support from an Nvidia RTX 4090 GPU.

4.5. Performance comparison

1) Quantitative Results

To validate the effectiveness of the proposed method, we compared its performance with selected mainstream adversarial attack methods across multiple model architectures, using attack success rate(ASR) as the evaluation metric. ASR refers to the proportion of images that successfully induce the model to make incorrect predictions among all attacked images. It is calculated as follows

$$\mathrm{ASR} = \frac{N_{\mathrm{error}}}{N_{\mathrm{total}}} \times 100\% \tag{14}$$

where N_{error} denotes the number of successful adversarial examples, and N_{total} denotes the total number of adversarial examples. A higher ASR indicates a more effective adversarial attack.

The comparison results on two datasets are presented in Table 2 and Table 3. In these tables, the first column represents the substitute model, the second column lists mainstream attack methods, and each subsequent column indicates the attack success rate of adversarial examples generated on the substitute model against the corresponding target model. For the MTARSI dataset, due to identical dataset splits, we directly used the experimental data from SFCoT [3]. For the FGSCR-42 dataset, due to differences in dataset splits, we re-conducted experiments for all comparison methods using their recommended configurations to ensure fairness.

The results demonstrate that our method significantly outperforms state-of-the-art approaches across different models. On the FGSCR-42 dataset (Table 2), Compared with the best performance among all comparison methods, our approach achieves an average improvement of 8.84% and a maximum improvement of 25.81% in black-box ASR. In same-architecture attacks between VGG-16 and VGG-19, and between ResNet-18 and ResNet-50, we achieved a 100% ASR. When using Inception-ResNet-v2 as a surrogate model, the highest average black-box ASR was

achieved, reaching 14.92%. When using DenseNet-121 as a surrogate model to attack the VGG19 architecture, we achieved the highest ASR improvement, reaching 25.81%. On the MTARSI dataset (Table 3), compared with the best performance among all comparison methods, our approach achieves an average improvement of 12.15% and a maximum improvement of 32.28% in black-box ASR. When using ResNet-18 and ResNet-50 architectures as surrogate models, we achieved the highest average black-box ASR improvements compared to all comparison methods, with improvements of 17.14% and 17.43% respectively. Particularly, when ResNet-50 attacks Inception-ResNet-v2, it achieved a 32.28% improvement compared to state-of-the-art performance. Overall, the results demonstrate the superior performance of our method against heterogeneous architectures, consistently outperforming state-of-the-art techniques. Table 4 shows the adversarial examples generated by different attack methods, which have minimal visual differences compared to the original examples.

2) Computational Complexity

This paper compares the time complexity of the proposed method with other input transformation-based attack methods. The experiment was conducted using Resnet-34 as the substitute model on the MTARSI dataset. We compared the time consumption and overall attack success rate (OASR) of the methods, where OASR is defined as the average ASR of adversarial examples across multiple black-box models. According to the results shown in Table 5, our method reaches an OASR of 90.4, delivering a 38.4% improvement over Admix while consuming a similar amount of time. These experimental results show that the proposed method achieves a favorable balance between efficiency and effectiveness.

4.6. Ablation Studies

To explore the impact of different mixing strategies on attack transferability, we designed an ablation study specifically targeting input transformation components. We propose Local Mix, a local mixing strategy that enhances adversarial examples by mixing different images at localized regions. To verify the contribution of our input transformation to transferability, we further designed a comparison baseline by replacing our transformation pipeline with Admix, where two different images are globally mixed, while keeping all other loss terms unchanged. No Mix refers to a baseline setting where no input transformation or mixing techniques are applied. As shown in the Table 6 and Table 7, our Local Mix strategy achieves higher attack success rates than both Admix and No Mix baselines in most cases. This focused analysis demonstrates the effectiveness of our proposed local mixing approach for improving adversarial transferability.

Furthermore, to analyze the contribution of the proposed loss function to attack performance, we conducted an additional ablation study on the loss components. Our method jointly optimizes the gradient direction using both a logit loss and a perturbation smoothing loss. Table 8 and Table 9 illustrates the attack success rates when using Dense-121 and Inception-ResNet-v2 as substitute models against various target models. Specifically, "All" denotes the full loss combination, "w/o Smo." indicates the removal of the perturbation smoothing loss and "CE only" refers to using the cross-entropy loss. The results show that removing the perturbation smoothing loss leads to a significant performance drop, especially when attacking Inception-ResNet-v2, highlighting its importance in enhancing transferability to heterogeneous models. When using only cross-entropy loss, performance further degrades, demonstrating its limited effectiveness in improving transferability. These results demonstrate the superiority of the proposed loss function over traditional cross entropy loss. The logit loss helps avoid gradient vanishing and guides more effective perturbation directions, while the perturbation smoothing loss suppresses high-frequency noise, thereby enhancing adversarial transferability across diverse model architectures.

4.7. Parameter Analysis

This section analyzes the parameters used in the experiments, which include the transformation times M, the loss weight λ, and the image mixing ratio η. The parameter experiments were conducted on FGSCR-42 using ResNet-34 as the substitute model.

Fig. 3 illustrates the effect of the input transformation times M on the attack success rate across different models. As M increases from 5 to 25, the attack success rate consistently improves, especially for models like Inception-ResNet-V2 that are harder to attack in the black-box setting. Beyond M=25, the improvements tend to plateau for most models, suggesting diminishing returns. Considering this trade-off between attack effectiveness and computational overhead, we choose M=25 as a balanced setting. It ensures strong transferability while avoiding unnecessary computation from excessive transformations.

Fig. 5 demonstrates the effect of varying the mixing ratio η on attack success rate. When $\eta = 0$, the method reverts to not applying any mixing, resulting in the lowest attack success rate. The highest attack success rate is achieved when $\eta = 0.5$, indicating that a moderate mixing ratio optimizes performance.

To determine the optimal λ parameter, we conducted sensitivity experiments on the MTARSI dataset using ResNet-34 as the white-box surrogate model, evaluating the impact of different λ values on attack success rates (ASR) across six target models. As shown in the Fig. 4, VGG series, ResNet series, and DenseNet-121 models maintained high ASR above 90% from $\lambda = 0$ to $\lambda = 200$, but performance began to decline when $\lambda > 200$. In contrast, Inception-ResNet-V2 exhibited the opposite trend: ASR was only 47% at $\lambda = 0$ but improved significantly as λ increased, reaching 75% at $\lambda = 400$. This phenomenon may be attributed to Inception-ResNet-V2's unique network architecture. Considering the overall performance across all models, we selected $\lambda = 200$ as the optimal parameter, which maintains high attack

Table 2
Attack Success Rates (%) on FGSCR-42 Dataset, ↑ indicates performance improvement over the best baseline.

Model	Attack	Vgg-16	Vgg-19	Res-34	Res-50	Dense-121	IncRes-v2
Vgg-16	PGD	100.00	99.25	75.77	87.26	78.85	38.13
	MIM	99.25	98.66	78.93	87.34	82.26	49.70
	PIM	100.00	99.16	75.52	87.17	81.84	41.38
	TIM	100.00	99.83	67.02	71.19	69.85	30.72
	DIM	100.00	100.00	94.69	91.42	89.34	36.30
	SIM	100.00	100.00	82.68	92.17	90.09	37.63
	Admix	100.00	99.50	82.09	91.09	87.51	51.54
	Mixup	90.59	90.59	82.09	87.76	82.01	52.45
	Mixcut	100.00	100.00	88.75	84.83	93.67	53.20
	SSA	99.16	97.83	76.51	83.93	80.01	48.62
	BSR	99.91	99.83	87.09	93.33	92.08	48.04
	SFCoT	100.00	99.91	94.50	97.08	95.17	52.20
	Ours	**100.00** (0.00↑)	**100.00** (0.00↑)	**99.33** (4.64↑)	**99.33** (2.25↑)	**98.33** (3.16↑)	**60.36** (7.16↑)
Vgg-19	PGD	97.16	100.00	71.27	85.17	80.51	36.55
	MIM	97.50	99.08	74.85	86.01	82.26	48.62
	PIM	97.83	100.00	74.68	86.76	81.76	40.21
	TIM	92.58	100.00	66.44	68.02	68.44	31.05
	DIM	99.50	100.00	82.26	90.50	89.17	37.13
	SIM	99.33	100.00	81.68	89.09	88.25	36.80
	Admix	98.91	100.00	82.18	89.67	86.92	50.70
	Mixup	92.50	90.75	79.93	87.76	84.09	51.70
	Mixcut	99.66	100.00	88.00	92.58	91.42	51.20
	SSA	96.31	90.16	72.77	84.09	79.51	46.71
	BSR	99.41	100.00	83.68	91.09	90.92	45.71
	SFCoT	99.83	100.00	89.17	94.92	94.25	48.62
	Ours	**100.00** (0.17↑)	**100.00** (0.00↑)	**97.58** (8.41↑)	**98.58** (3.66↑)	**98.33** (4.08↑)	**53.03** (1.33↑)
Res-34	PGD	18.23	11.15	100.00	68.44	49.04	32.47
	MIM	56.28	35.97	100.00	78.01	66.77	53.78
	PIM	39.38	21.89	100.00	71.94	60.03	39.05
	TIM	16.31	7.16	100.00	43.37	88.80	17.65
	DIM	44.79	30.39	100.00	83.68	75.27	27.56
	SIM	43.79	28.97	100.00	84.76	75.60	27.89
	Admix	74.68	62.53	100.00	88.42	85.67	55.62
	Mixup	77.10	64.44	98.08	88.84	84.42	54.45
	Mixcut	79.01	67.44	100.00	93.08	90.34	55.95
	SSA	67.77	57.45	100.00	93.42	84.42	51.70
	BSR	80.34	69.27	100.00	97.16	94.17	54.62
	SFCoT	88.42	79.01	100.00	99.41	97.75	55.70
	Ours	**97.83** (9.41↑)	**95.50** (16.49↑)	**100.00** (0.00↑)	**100.00** (0.59↑)	**99.58** (1.83↑)	**68.44** (12.49↑)
Res-50	PGD	17.23	10.15	57.86	100.00	53.37	32.30
	MIM	51.45	32.80	72.10	100.00	71.35	53.78
	PIM	33.88	19.73	69.60	100.00	67.61	37.80
	TIM	15.65	7.74	45.87	100.00	45.87	16.98
	DIM	41.38	30.72	85.76	100.00	90.09	28.72
	SIM	42.71	30.55	94.09	100.00	90.75	28.89
	Admix	72.68	60.86	91.09	100.00	91.50	54.62
	Mixup	74.52	62.61	88.84	97.58	88.09	55.87
	Mixcut	73.18	62.94	94.00	100.00	94.25	55.53
	SSA	68.10	58.86	90.25	100.00	89.67	50.70
	BSR	73.43	62.44	95.75	100.00	98.91	53.37
	SFCoT	81.01	73.68	98.50	100.00	99.16	54.53
	Ours	**97.58** (16.57↑)	**96.50** (22.82↑)	**100.00** (1.50↑)	**100.00** (0.00↑)	**100.00** (0.84↑)	**68.85** (12.98↑)
Dense-121	PGD	21.23	14.32	56.53	72.43	100.00	32.72
	MIM	57.86	42.96	72.18	83.76	100.00	53.28
	PIM	41.38	28.80	71.94	82.68	100.00	40.21
	TIM	18.15	8.74	46.71	51.12	100.00	18.23
	DIM	46.79	34.30	81.84	92.00	100.00	27.81
	SIM	45.96	34.97	80.59	91.75	100.00	28.97
	Admix	76.18	65.69	86.34	89.75	100.00	54.28
	Mixup	78.68	65.44	84.92	87.59	97.41	54.03
	Mixcut	78.01	66.27	88.92	92.58	100.00	54.78
	SSA	66.11	60.11	81.59	89.84	100.00	50.54
	BSR	74.00	63.28	90.42	94.92	100.00	52.87
	SFCoT	81.34	70.94	95.50	99.80	100.00	53.03
	Ours	**96.75** (15.41↑)	**96.75** (25.81↑)	**99.66** (4.16↑)	**99.83** (0.03↑)	**100.00** (0.00↑)	**69.60** (14.82↑)
IncRes-v2	PGD	4.99	3.49	16.31	29.05	20.23	100.00
	MIM	11.90	7.32	24.97	37.30	32.22	100.00
	PIM	5.91	3.66	17.98	29.72	22.31	100.00
	TIM	6.91	3.83	20.31	21.48	17.06	100.00
	DIM	12.15	5.74	28.39	37.88	33.13	100.00
	SIM	12.23	5.66	27.56	37.80	31.72	100.00
	Admix	16.98	7.91	30.64	41.46	41.13	99.91
	Mixup	19.23	8.65	29.47	42.38	42.54	96.83
	Mixcut	18.98	9.65	30.55	44.46	40.96	100.00
	SSA	14.15	6.91	26.64	37.13	31.80	100.00
	BSR	29.05	13.32	42.21	51.54	45.21	100.00
	SFCoT	30.39	13.40	40.04	46.87	41.93	99.91
	Ours	**44.54** (14.15↑)	**24.31** (10.91↑)	**56.36** (14.15↑)	**69.19** (17.65↑)	**62.94** (17.73↑)	**100.00** (0.00↑)

Table 3
Attack Success Rates (%) on MTARSI Dataset, ↑ indicates performance improvement over the best baseline.

Model	Attack	Vgg-16	Vgg-19	Res-34	Res-50	Dense-121	IncRes-v2
Vgg-16	PGD	100.0	64.7	20.3	22.5	28.3	8.4
	MIM	99.9	93.6	47.8	51.3	60.4	29.7
	PIM	100.0	93.4	48.5	53.0	58.8	25.2
	TIM	100.0	87.2	45.4	50.7	52.8	19.5
	DIM	100.0	97.3	61.6	65.8	69.2	32.8
	SIM	100.0	96.6	47.5	53.5	63.2	30.4
	Admix	100.0	98.6	56.8	60.4	68.8	32.1
	Mixup	99.8	97.9	50.8	54.6	66.0	30.6
	Mixcut	97.3	98.2	53.1	57.4	66.4	30.7
	SSA	100.0	95.3	51.5	55.2	62.7	28.3
	BSR	100.0	99.4	65.6	70.1	78.0	33.2
	SFCoT	100.0	99.9	77.1	81.9	87.2	34.7
	Ours	**100.00** (0.00↑)	**100.00** (0.10↑)	**90.40** (13.30↑)	**91.76** (9.86↑)	**94.28** (7.08↑)	**52.59** (17.89↑)
Vgg-19	PGD	61.3	100.0	18.9	20.3	27.9	7.8
	MIM	94.8	99.9	48.3	52.5	59.8	25.4
	PIM	94.7	100.0	50.7	51.5	58.0	22.2
	TIM	85.2	100.0	44.8	52.1	52.6	15.5
	DIM	98.1	99.9	59.0	63.6	69.6	30.4
	SIM	97.8	100.0	52.0	58.2	73.9	25.1
	Admix	99.7	100.0	62.0	64.9	70.9	26.2
	Mixup	98.6	99.1	55.5	60.3	67.0	24.5
	Mixcut	98.9	99.4	54.7	59.2	67.3	25.1
	SSA	96.7	99.9	52.6	53.8	63.4	27.7
	BSR	99.8	100.0	66.6	71.1	77.6	30.5
	SFCoT	100.0	100.0	76.7	81.5	88.5	31.2
	Ours	**100.00** (0.00↑)	**100.00** (0.00↑)	**92.13** (15.43↑)	**92.97** (11.47↑)	**96.11** (7.61↑)	**47.71** (16.51↑)
Res-34	PGD	4.1	3.8	75.8	12.3	9.3	7.4
	MIM	27.0	27.9	100.0	43.4	47.9	31.2
	PIM	18.6	20.2	99.9	40.9	41.1	20.1
	TIM	3.1	2.4	100.0	19.6	16.3	2.7
	DIM	44.9	45.5	99.9	68.4	68.3	33.8
	SIM	38.5	38.9	99.8	48.1	51.3	25.8
	Admix	49.4	49.1	100.0	64.3	66.2	31.3
	Mixup	40.9	40.8	92.9	55.4	60.4	28.3
	Mixcut	38.2	40.9	99.7	55.4	59.4	28.5
	SSA	51.4	51.8	99.9	65.5	64.6	29.8
	BSR	68.7	68.0	100.0	88.8	84.6	35.8
	SFCoT	77.2	75.5	100.0	91.6	86.0	32.4
	Ours	**94.38** (17.18↑)	**93.65** (18.15↑)	**100.00** (0.00↑)	**97.74** (6.14↑)	**99.10** (13.10↑)	**66.91** (31.11↑)
Res-50	PGD	4.9	5.0	11.5	66.6	8.7	7.3
	MIM	22.1	23.4	41.2	99.8	45.9	25.9
	PIM	15.8	17.1	37.7	99.2	39.0	17.1
	TIM	2.7	2.9	16.0	99.0	15.9	1.7
	DIM	42.9	43.0	67.4	99.8	71.6	28.0
	SIM	31.2	29.2	38.7	93.4	46.2	21.3
	Admix	43.0	42.2	55.7	99.6	66.7	25.9
	Mixup	34.6	34.9	46.3	94.7	57.8	23.7
	Mixcut	33.7	34.3	45.1	98.6	57.4	23.6
	SSA	50.1	52.2	65.6	99.7	64.6	23.7
	BSR	59.8	61.0	81.2	100.0	82.2	28.3
	SFCoT	76.0	75.7	91.1	100.0	89.6	28.6
	Ours	**95.22** (19.22↑)	**93.49** (17.79↑)	**99.42** (8.32↑)	**100.00** (0.00↑)	**99.16** (9.56↑)	**60.88** (32.28↑)
Dense-121	PGD	5.4	5.2	12.6	12.7	78.3	8.2
	MIM	26.9	28.1	38.0	38.6	99.9	28.9
	PIM	21.8	22.0	37.5	40.0	99.9	19.2
	TIM	3.4	3.5	14.5	18.9	99.9	3.0
	DIM	48.0	49.1	61.6	63.4	99.9	33.4
	SIM	32.0	33.7	37.8	41.6	99.8	25.2
	Admix	43.9	47.9	54.9	57.7	100.0	30.8
	Mixup	34.8	38.5	45.1	49.4	96.0	28.3
	Mixcut	34.4	37.8	46.3	47.5	91.6	28.0
	SSA	49.1	55.1	60.3	63.9	99.9	29.2
	BSR	64.3	64.2	73.2	79.7	100.0	35.0
	SFCoT	81.7	82.3	88.4	91.9	100.0	33.0
	Ours	**94.96** (13.26↑)	**96.64** (14.34↑)	**99.00** (10.60↑)	**97.11** (5.21↑)	**100.00** (0.00↑)	**67.22** (32.22↑)
IncRes-v2	PGD	2.8	2.7	5.3	6.2	4.6	58.7
	MIM	4.3	5.0	7.8	8.8	7.6	100.0
	PIM	4.7	4.9	8.0	9.1	8.5	100.0
	TIM	1.3	1.1	3.3	4.2	3.6	100.0
	DIM	6.6	7.8	12.8	15.6	13.9	100.0
	SIM	4.3	5.4	6.2	8.3	7.6	62.3
	Admix	4.9	5.5	8.5	9.7	8.4	87.4
	Mixup	3.7	4.3	6.9	6.7	7.2	96.5
	Mixcut	4.1	4.3	6.8	6.5	7.4	96.6
	SSA	4.9	5.5	9.0	10.2	8.6	98.1
	BSR	7.9	9.5	13.5	16.7	14.2	100.0
	SFCoT	9.7	11.2	13.6	19.1	17.8	100.0
	Ours	**11.64** (1.94↑)	**11.74** (0.54↑)	**21.23** (7.63↑)	**23.59** (4.49↑)	**19.97** (2.17↑)	**100.00** (0.00↑)

Table 4
Comparison of the adversarial examples generated by different methods with the original images.

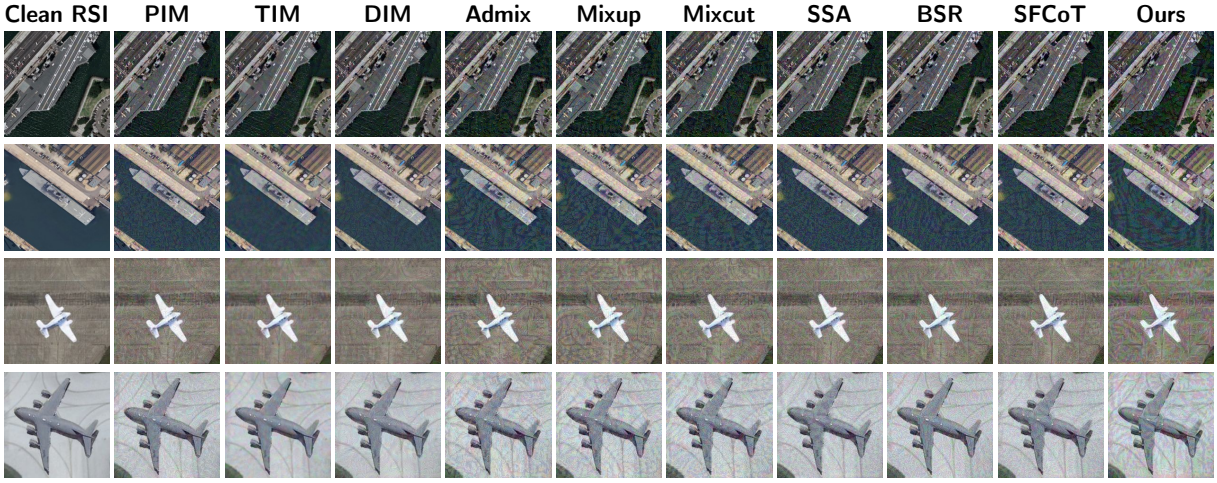

Table 5
Comparison of Computational Complexity and Overall Attack Success Rate.

	SIM	Admix	SSA	BSR	SFCoT	**Ours**
Time (s)	785	2075	453	214	399	2130
OSAR	40.5	52.0	52.6	69.1	72.5	90.4

Table 6
Ablation study of different mix strategies across various models on FGSCR-42.

Model	Mix Strategy	Vgg-19	Res-34	Dense-121	IncRes-v2
Vgg-19	Local-Mix	100.00	97.58	98.33	53.03
	Admix	100.00	96.39	97.45	52.83
	No-Mix	100.00	95.50	97.00	51.20
Res-34	Local-Mix	95.50	100.00	99.58	68.44
	Admix	92.45	100.00	99.17	67.26
	No-Mix	88.92	100.00	98.83	63.28
Dense-121	Local-Mix	96.75	99.66	100.00	69.60
	Admix	93.76	97.94	99.83	68.00
	No-Mix	91.67	97.33	100.00	63.86

success rates for most models while avoiding performance degradation at higher λ values.

5. Conclusion

This paper proposes a novel adversarial attack method to address the challenge of generating transferable adversarial examples in remote sensing object recognition. Unlike existing mixing based attack methods to enhance transferability, which either perform global blending or directly exchange a region in the images, we present a local mixing strategy to generate diverse yet semantically consistent inputs during the generation of adversarial examples. The proposed local mixing method merely blends local regions of two images to preserve as much of the global semantic information as possible. Moreover, unlike traditional cross-entropy loss, we design an untargeted attack loss based on logits optimization, which mitigates the gradient vanishing problem inherent to

Table 7
Ablation study of different mix strategies across various models on MTARSI.

Model	Mix Strategy	Vgg-19	Res-34	Dense-121	IncRes-v2
Vgg-19	Local-Mix	100.00	92.13	96.11	47.71
	Admix	100.00	90.50	96.80	45.51
	No-Mix	100.00	88.98	95.85	41.95
Res-34	Local-Mix	93.65	100.00	99.91	66.91
	Admix	90.03	100.00	96.38	57.89
	No-Mix	87.46	100.00	97.01	55.79
Dense-121	Local-Mix	96.64	99.00	100.00	67.22
	Admix	96.59	98.37	100.00	62.71
	No-Mix	94.17	95.64	100.00	58.04

Table 8
Ablation study of different loss function components when using Inception-ResNet-v2 as substitute model on FGSCR-42 dataset.

Loss	Vgg-16	Vgg-19	Res-34	Res-50	Dense-121
All	44.54	24.31	56.36	69.19	62.94
w/o Smo.	34.47	18.56	48.95	62.36	56.53
only CE	31.14	16.56	48.79	62.19	57.78

Table 9
Ablation study of different loss function components when using Dense-121 as substitute model on FGSCR-42 dataset.

Loss	Vgg-16	Vgg-19	Res-34	Res-50	IncRes-v2
All	97.08	96.83	99.50	99.66	69.85
w/o Smo.	96.16	96.25	99.41	99.83	60.53
only CE	91.00	88.17	98.66	99.58	59.45

cross entropy loss and constrains the high-frequency components generated during the gradient update process, further enhancing transferability across heterogeneous architectures. Experimental results on the FGSCR-42 and MTARSI datasets show that our method outperforms existing techniques in both attack performance and transferability, effectively improving the attack's effectiveness across multiple model architectures.

References

[1] Gencer Sumbul, Ramazan Gokberk Cinbis, and Selim Aksoy. Fine-grained object recognition and zero-shot learning in remote sensing imagery. *IEEE Transactions on Geoscience and Remote Sensing*, 56(2):770–779, 2017.

[2] Yimin Fu, Zhunga Liu, and Zuowei Zhang. Progressive learning vision transformer for open set recognition of fine-grained objects in remote sensing images. *IEEE Transactions on Geoscience and Remote Sensing*, 61:1–13, 2023.

[3] Yimin Fu, Zhunga Liu, and Jialin Lyu. Transferable adversarial attacks for remote sensing object recognition via spatial-frequency co-transformation. *IEEE Transactions on Geoscience and Remote Sensing*, 2024.

[4] Ian J Goodfellow, Jonathon Shlens, and Christian Szegedy. Explaining and harnessing adversarial examples. *arXiv preprint arXiv:1412.6572*, 2014.

[5] Alexey Kurakin, Ian J Goodfellow, and Samy Bengio. Adversarial examples in the physical world. In *Artificial intelligence safety and security*, pages 99–112. Chapman and Hall/CRC, 2018.

[6] Ian J Goodfellow, Jonathon Shlens, and Christian Szegedy. Explaining and harnessing adversarial examples. *arXiv preprint arXiv:1412.6572*, 2014.

[7] Aleksander Madry, Aleksandar Makelov, Ludwig Schmidt, Dimitris Tsipras, and Adrian Vladu. Towards deep learning models resistant to adversarial attacks. *arXiv preprint arXiv:1706.06083*, 2017.

[8] Cihang Xie, Zhishuai Zhang, Yuyin Zhou, Song Bai, Jianyu Wang, Zhou Ren, and Alan L Yuille. Improving transferability of adversarial examples with input diversity. In *Proceedings of the IEEE/CVF conference on computer vision and pattern recognition*, pages 2730–2739, 2019.

[9] Lianli Gao, Qilong Zhang, Jingkuan Song, Xianglong Liu, and Heng Tao Shen. Patch-wise attack for fooling deep neural network. In *Computer Vision–ECCV 2020: 16th European Conference, Glasgow, UK, August 23–28, 2020, Proceedings, Part XXVIII 16*, pages 307–322. Springer, 2020.

[10] Yinpeng Dong, Tianyu Pang, Hang Su, and Jun Zhu. Evading defenses to transferable adversarial examples by translation-invariant attacks. In *Proceedings of the IEEE/CVF conference on computer vision and pattern recognition*, pages 4312–4321, 2019.

[11] Jiadong Lin, Chuanbiao Song, Kun He, Liwei Wang, and John E Hopcroft. Nesterov accelerated gradient and scale invariance for adversarial attacks. *arXiv preprint arXiv:1908.06281*, 2019.

[12] Yuyang Long, Qilong Zhang, Boheng Zeng, Lianli Gao, Xianglong Liu, Jian Zhang, and Jingkuan Song. Frequency domain model augmentation for adversarial attack. In *European conference on computer vision*, pages 549–566. Springer, 2022.

[13] Yinpeng Dong, Fangzhou Liao, Tianyu Pang, Hang Su, Jun Zhu, Xiaolin Hu, and Jianguo Li. Boosting adversarial attacks with momentum. In *Proceedings of the IEEE conference on computer vision and pattern recognition*, pages 9185–9193, 2018.

[14] Yanpei Liu, Xinyun Chen, Chang Liu, and Dawn Song. Delving into transferable adversarial examples and black-box attacks. *arXiv preprint arXiv:1611.02770*, 2016.

[15] Wen Zhou, Xin Hou, Yongjun Chen, Mengyun Tang, Xiangqi Huang, Xiang Gan, and Yong Yang. Transferable adversarial perturbations. In *Proceedings of the European Conference on Computer Vision (ECCV)*, pages 452–467, 2018.

[16] Xinlong Ding, Jiansheng Chen, Hongwei Yu, Yu Shang, Yining Qin, and Huimin Ma. Transferable adversarial attacks for object detection using object-aware significant feature distortion. In *Proceedings of the AAAI Conference on Artificial Intelligence*, volume 38, pages 1546–1554, 2024.

[17] Junlin Liu, Chenyu Zhang, and Xinchen Lyu. Boosting the transferability of adversarial examples via local mixup and adaptive step size. In *ICASSP 2025-2025 IEEE International Conference on Acoustics, Speech and Signal Processing (ICASSP)*, pages 1–5. IEEE, 2025.

[18] Maosen Li, Cheng Deng, Tengjiao Li, Junchi Yan, Xinbo Gao, and Heng Huang. Towards transferable targeted attack. In *Proceedings of the IEEE/CVF conference on computer vision and pattern recognition*, pages 641–649, 2020.

[19] Li Chen, Zewei Xu, Qi Li, Jian Peng, Shaowen Wang, and Haifeng Li. An empirical study of adversarial examples on remote sensing image scene classification. *IEEE Transactions on Geoscience and Remote Sensing*, 59(9):7419–7433, 2021.

[20] Yonghao Xu, Bo Du, and Liangpei Zhang. Assessing the threat of adversarial examples on deep neural networks for remote sensing scene classification: Attacks and defenses. *IEEE Transactions on Geoscience and Remote Sensing*, 59(2):1604–1617, 2020.

[21] Li Chen, Zewei Xu, Qi Li, Jian Peng, Shaowen Wang, and Haifeng Li. An empirical study of adversarial examples on remote sensing image scene classification. *IEEE Transactions on Geoscience and Remote Sensing*, 59(9):7419–7433, 2021.

[22] Cheng Shi, Yenan Dang, Li Fang, Minghua Zhao, Zhiyong Lv, Qiguang Miao, and Chi-Man Pun. Multifeature collaborative adversarial attack in multimodal remote sensing image classification. *IEEE Transactions on Geoscience and Remote Sensing*, 60:1–15, 2022.

[23] Yonghao Xu and Pedram Ghamisi. Universal adversarial examples in remote sensing: Methodology and benchmark. *IEEE Transactions on Geoscience and Remote Sensing*, 60:1–15, 2022.

[24] Xiaosen Wang, Xuanran He, Jingdong Wang, and Kun He. Admix: Enhancing the transferability of adversarial attacks. In *Proceedings of the IEEE/CVF international conference on computer vision*, pages 16158–16167, 2021.

[25] Zhengyu Zhao, Zhuoran Liu, and Martha Larson. On success and simplicity: A second look at transferable targeted attacks. *Advances in Neural Information Processing Systems*, 34:6115–6128, 2021.

[26] Li Li, Miloš Doroslovački, and Murray H Loew. Approximating the gradient of cross-entropy loss function. *IEEE access*, 8:111626–111635, 2020.

[27] Battista Biggio and Fabio Roli. Wild patterns: Ten years after the rise of adversarial machine learning. In *Proceedings of the 2018 ACM SIGSAC Conference on Computer and Communications Security*, pages 2154–2156, 2018.

[28] Aleksander Madry, Aleksandar Makelov, Ludwig Schmidt, Dimitris Tsipras, and Adrian Vladu. Towards deep learning models resistant to adversarial attacks. *arXiv preprint arXiv:1706.06083*, 2017.

[29] Nicolas Papernot, Patrick McDaniel, Ian Goodfellow, Somesh Jha, Z Berkay Celik, and Ananthram Swami. Practical black-box attacks against machine learning. In *Proceedings of the 2017 ACM on Asia conference on computer and communications security*, pages 506–519, 2017.

[30] Wieland Brendel, Jonas Rauber, and Matthias Bethge. Decision-based adversarial attacks: Reliable attacks against black-box machine learning models. *arXiv preprint arXiv:1712.04248*, 2017.

[31] Kunyu Wang, Xuanran He, Wenxuan Wang, and Xiaosen Wang. Boosting adversarial transferability by block shuffle and rotation. In *Proceedings of the IEEE/CVF Conference on Computer Vision and Pattern Recognition*, pages 24336–24346, 2024.

[32] Nicolas Papernot, Patrick McDaniel, Xi Wu, Somesh Jha, and Ananthram Swami. Distillation as a defense to adversarial perturbations against deep neural networks. In *2016 IEEE symposium on security and privacy (SP)*, pages 582–597. IEEE, 2016.

[33] Sravanti Addepalli, Vivek BS, Arya Baburaj, Gaurang Sriramanan, and R Venkatesh Babu. Towards achieving adversarial robustness by enforcing feature consistency across bit planes. In *Proceedings of the*

IEEE/CVF conference on computer vision and pattern recognition, pages 1020–1029, 2020.

[34] Hengrui Liao and Yue Li. Lfc-unet: learned lossless medical image fast compression with u-net. *PeerJ Computer Science*, 10:e1924, 2024.

[35] Florian Tramèr, Alexey Kurakin, Nicolas Papernot, Ian Goodfellow, Dan Boneh, and Patrick McDaniel. Ensemble adversarial training: Attacks and defenses. *arXiv preprint arXiv:1705.07204*, 2017.

[36] Harini Kannan, Alexey Kurakin, and Ian Goodfellow. Adversarial logit pairing. *arXiv preprint arXiv:1803.06373*, 2018.

[37] Chuan Guo, Mayank Rana, Moustapha Cisse, and Laurens Van Der Maaten. Countering adversarial images using input transformations. *arXiv preprint arXiv:1711.00117*, 2017.

[38] Cihang Xie, Jianyu Wang, Zhishuai Zhang, Zhou Ren, and Alan Yuille. Mitigating adversarial effects through randomization. *arXiv preprint arXiv:1711.01991*, 2017.

[39] Shiwei Shen, Guoqing Jin, Ke Gao, and Yongdong Zhang. Ape-gan: Adversarial perturbation elimination with gan. *arXiv preprint arXiv:1707.05474*, 2017.

[40] Yanghua Di, Zhiguo Jiang, and Haopeng Zhang. A public dataset for fine-grained ship classification in optical remote sensing images. *Remote Sensing*, 13(4):747, 2021.

[41] Zhi-Ze Wu, Shou-Hong Wan, Xiao-Feng Wang, Ming Tan, Le Zou, Xin-Lu Li, and Yan Chen. A benchmark data set for aircraft type recognition from remote sensing images. *Applied Soft Computing*, 89:106132, 2020.

[42] Karen Simonyan and Andrew Zisserman. Very deep convolutional networks for large-scale image recognition. *arXiv preprint arXiv:1409.1556*, 2014.

[43] Kaiming He, Xiangyu Zhang, Shaoqing Ren, and Jian Sun. Deep residual learning for image recognition. In *Proceedings of the IEEE conference on computer vision and pattern recognition*, pages 770–778, 2016.

[44] Gao Huang, Zhuang Liu, Laurens Van Der Maaten, and Kilian Q Weinberger. Densely connected convolutional networks. In *Proceedings of the IEEE conference on computer vision and pattern recognition*, pages 4700–4708, 2017.

[45] Christian Szegedy, Sergey Ioffe, Vincent Vanhoucke, and Alexander Alemi. Inception-v4, inception-resnet and the impact of residual connections on learning. In *Proceedings of the AAAI conference on artificial intelligence*, volume 31, 2017.

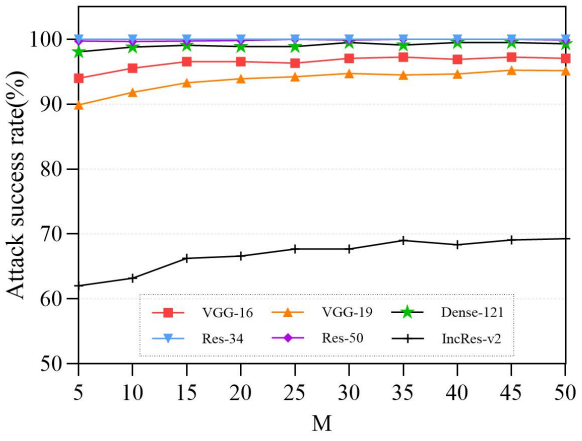

Figure 3: Attack success rate with different settings M .

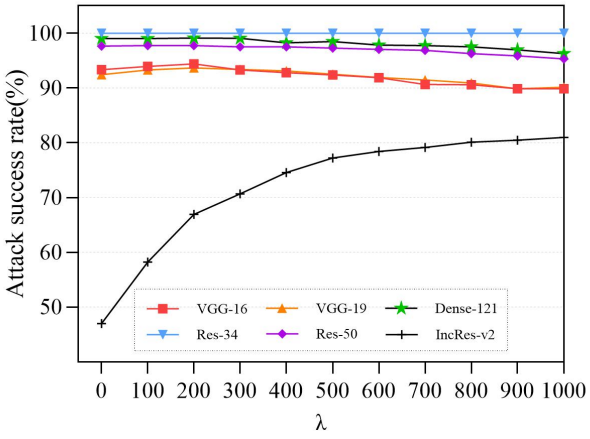

Figure 4: Attack success rate with different settings of λ .

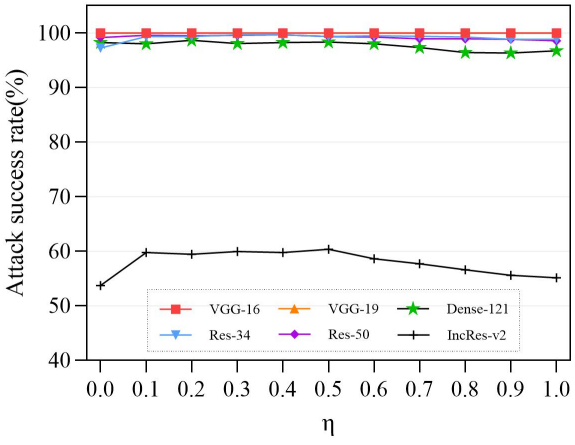

Figure 5: Attack success rate with different settings of η .